Cell

Structural Memory in the Contractile Ring Makes the Duration of Cytokinesis Independent of Cell Size

Ana Carvalho,[1,*] Arshad Desai,[1] and Karen Oegema[1,*]
[1]Ludwig Institute for Cancer Research, Department of Cellular and Molecular Medicine, University of California, San Diego, CMM-East 3080, 9500 Gilman Drive, La Jolla, CA 92093, USA
*Correspondence: ancarvalho@ucsd.edu (A.C.), koegema@ucsd.edu (K.O.)
DOI 10.1016/j.cell.2009.03.021

SUMMARY

Cytokinesis is accomplished by constriction of a cortical contractile ring. We show that during the early embryonic divisions in *C. elegans*, ring constriction occurs in two phases—an initial phase at a constant rate followed by a second phase during which the constriction rate decreases in proportion to ring perimeter. Cytokinesis completes in the same amount of time, despite the reduction in cell size during successive divisions, due to a strict proportionality between initial ring size and the constant constriction rate. During closure, the myosin motor in the ring decreases in proportion to perimeter without turning over. We propose a "contractile unit" model to explain how the ring retains a structural memory of its initial size as it disassembles. The scalability of constriction may facilitate coordination of mitotic events and cytokinesis when cell size, and hence the distance traversed by the ring, varies during embryogenesis and in other contexts.

INTRODUCTION

In animal cells, cytokinesis is accomplished by constriction of a cortical contractile ring. Contractile rings are composed of a network of protein polymers that includes actin filaments, bipolar filaments of the motor myosin II, and septin filaments. Contractile rings also contain the crosslinker anillin, which binds directly to all three filament types, and proteins that regulate actin nucleation, capping, polymerization, disassembly, and crosslinking (Eggert et al., 2006; Field et al., 2008; Wu and Pollard, 2005).

Understanding the structural organization of the contractile ring and how it generates contractile stress is an important current challenge. Based on analogy to muscle, it has been proposed that contractile stress is generated via a "sliding filament" mechanism in which bipolar myosin filaments walk along actin filaments within organized sarcomere-like arrays (Schroeder, 1975). The contractile ring has been examined by electron microscopy (EM) in a variety of experimental systems, including several marine invertebrates, newts, vertebrate cultured cells, fission yeast, and the single-celled ciliate *Nassula* (Schroeder, 1968, 1970, 1972; Selman and Perry, 1970; Arnold, 1969; Tucker, 1971; Maupin and Pollard, 1986; Kamasaki et al., 2007). In all cases, a thin (0.1–0.2 μm) layer of circumferentially oriented actin filaments was observed directly beneath the plasma membrane. In contrast to the conserved thickness, the width of the actin layer along the plasma membrane was more variable between species (from <1 μm to ~20 μm). Myosin decoration indicates that the actin filaments within the contractile ring are of mixed polarity (Maupin and Pollard, 1986; Sanger and Sanger, 1980; Mabuchi et al., 1988; Kamasaki et al., 2007). However, organization of actin filaments into sarcomere-like arrays has not been reproducibly observed. In vitro studies and biophysical considerations have suggested two alternative mechanisms that would not require a sarcomere-like filament organization. In the first mechanism, myosin is proposed to generate contractile stress in the context of homogeneous bundles of actin filaments of random orientation (Takiguchi, 1991; Tanaka-Takiguchi et al., 2004; Kruse and Jülicher, 2000; Kruse et al., 2001; Kruse and Jülicher, 2003). In the second mechanism, contractile stress is proposed to arise from filament polymerization dynamics, in particular from actin filament depolymerization in the presence of end-tracking crosslinkers (Dogterom and Yurke, 1997; Mogilner and Oster, 2003; Dickinson et al., 2004; Zumdieck et al., 2007).

A second important question is what happens to the structure and components of the contractile ring as it constricts. In a classic EM study in sea urchin embryos, the volume of the actin filament network was found to decrease as constriction proceeded (Schroeder, 1972), indicating that the actin filaments disassemble as the ring gets smaller. EM analysis in the fission yeast *S. pombe* provided additional support for the idea that actin filaments shorten during ring constriction (Kamasaki et al., 2007). Analysis of GFP-tagged ring components in *S. pombe* has suggested that different contractile ring components have different fates—the total amount of the actin-associated proteins Rng2p, Cdc15p, Cdc12p, and Ain1p in the ring decreased in proportion to the decrease in ring circumference, whereas the total amount of myosin in the ring remained constant (Wu and Pollard, 2005). Fluorescence recovery after photobleaching (FRAP) studies on assembled rings in *S. pombe* revealed that Cdc4p (the myosin II essential light chain) and Cdc8p (the actin-associated protein tropomyosin) are both turning over rapidly ($t_{1/2}$ = 20–30 s; Pelham and Chang, 2002).

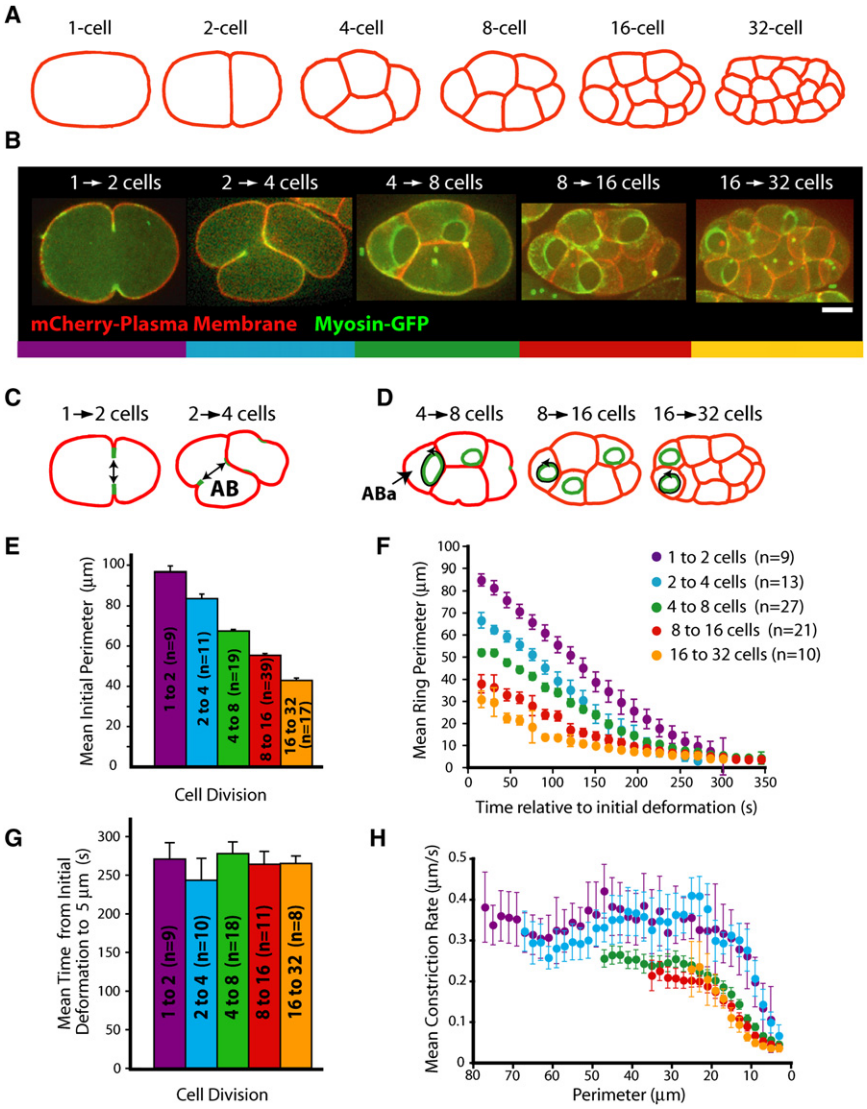

Figure 1. Monitoring Contractile Ring Closure during the First Five Divisions of the *C. elegans* Embryo

(A) Schematic outline of the cell boundaries in *C. elegans* embryos with 1, 2, 4, 8, 16, and 32 cells.

(B) Confocal images of embryos coexpressing NMY-2-GFP and an $RFP^{mCherry}$ plasma membrane probe. Scale bar, 10 μm.

(C) During the first two divisions, cells divide along axes parallel to the imaging plane. For consistency, all data for the 2→4 cell division was collected in the anterior AB cell.

(D) During the 4→8, 8→16, and 16→32 cell divisions, one or more cells typically divide along an axis perpendicular to the imaging plane. For the 4→8 cell division, all data were collected in the ABa cell; for the 8→16 and 16→32 cell stages, measurements from all vertically dividing cells gave indistinguishable results and were pooled.

(E) Mean initial perimeter, measured around the cell equator prior to constriction onset, for the first five cell divisions.

(F) Mean contractile ring perimeter plotted versus time after the initial deformation of the cortex.

(G) Mean duration of constriction, from the initial deformation of the cortex to a perimeter of 5 μm, for the first five cell divisions.

(H) Mean constriction rate plotted versus perimeter. The x-axis scale is reversed to represent progression from larger to smaller perimeters during constriction. Error bars, 95% CI.

A similar half-time has also been observed for labeled actin in the contractile ring in vertebrate cultured cells (Murthy and Wadsworth, 2005; Guha et al., 2005). These studies have led to the idea that contractile ring components turn over rapidly relative to the rate of constriction.

A major goal of studies of the contractile ring is to incorporate information on structure and component dynamics into a biophysical model that recapitulates the kinetics of constriction. In *S. pombe* and the amoebic parasite *E. invadens* the contractile ring constricts at a constant rate, leading to a linear decrease in ring perimeter with time (Pelham and Chang, 2002; Biron et al., 2004). During the first division of sea urchin and *C. elegans* embryos the contractile ring constricts at a constant rate for the majority (70%–90%) of constriction, after which the rate of constriction progressively slows (Mabuchi, 1994; Zumdieck et al., 2007). Attempts to generate a biophysical model that recapitulates a constant rate of closure have been based on different assumptions and have consequently led to substantially different ideas for how constriction may be achieved (Biron et al., 2005; He and Dembo, 1997; Zumdieck et al., 2007).

Here we explore the inherent properties of the contractile ring by monitoring the fate of ring components during constriction and investigating how constriction scales with respect to initial ring size in the *C. elegans* embryo. Our results establish that the contractile ring progressively disassembles while retaining a structural memory that renders constriction time independent of its initial size. This design principle explains how mitotic events and the duration of cytokinesis are coordinated when cell size varies during embryogenesis and in other biological contexts. We propose a ''contractile unit'' model that accounts for both the structural memory and the proportional decrease in ring components during constriction.

RESULTS

Contractile Ring Constricts in Two Phases Whose Relative Contributions Depend on Initial Ring Size

To investigate how cytokinesis scales with cell size, we measured the kinetics of contractile ring closure during the first five divisions of the *C. elegans* embryo. Constriction was monitored in embryos coexpressing an $RFP^{mCherry}$-labeled plasma membrane marker and a GFP fusion with the heavy chain of myosin II (NMY-2-GFP), which marks the contractile ring (Figures 1A and 1B). During the

first two divisions (1→2 and 2→4 cells), the cells divide parallel to the imaging plane, providing a side view of the contractile ring (Figure 1C and see Movie S1 available online). Because the contractile ring is circular during these divisions, ring perimeter was calculated from the diameter measured from a z-series acquired at each time point (see Supplemental Data A). During the subsequent three divisions (4→8, 8→16, and 16→32 cells), one or more cells divide along an axis perpendicular to the imaging plane, providing an "end-on" view of the ring (Figure 1D and Movie S2). During these divisions, the contractile ring is not a perfect circle due to the presence of cell-cell contacts, so the perimeter was measured by tracing the outline of the ring. In the early embryo, cell volume decreases ~2-fold during each sequential division; thus, the initial perimeter, measured prior to constriction onset, progressively decreases from ~100 μm at the first division to ~40 μm during the fifth division (Figure 1E).

We compared ring closure profiles for the different divisions by monitoring constriction in embryos (n = 9–27) for each division and plotting mean ring perimeter versus time (Figure 1F and Supplemental Data A and B). Times were assigned relative to the initial deformation of the cortex, which was the first point when a recognizable ingression was evident. The ring closure plots revealed that the duration of constriction is invariant between divisions (Figures 1F and 1G), implying that the larger rings in the earlier divisions constrict more rapidly than the smaller rings in later divisions. Plotting the constriction rate versus perimeter (Figure 1H and Supplemental Data C) revealed that ring closure occurs in two phases—an initial phase at a constant constriction rate, followed by a second phase during which the constriction rate decreased in proportion to perimeter. During each successive division, the percentage of closure accomplished at a constant rate decreased, until by the fifth division, the constriction rate decreased in proportion to perimeter from the first point where it could be accurately measured (Figure 1H and Supplemental Data D). Thus, during at least the first four embryonic divisions, contractile ring constriction occurs in two phases whose relative contributions change as a function of the initial size of the ring.

Transition from Constant to Decreasing Constriction Rate Occurs at a Fixed-Ring Perimeter and Requires the Spindle Midzone

To characterize the transition between the two phases of cytokinesis, we calculated the mean constriction rate during the constant phase and fit the last 6 (1→2 and 2→4 cells) or 9 (4→8 and 8→16 cells) data points, during which the rate of constriction was declining, to a linear trend. We defined the transition point as the perimeter when the value of the linear equation was equal to the mean constant phase constriction rate (Figure 2A and Supplemental Data D). This analysis revealed that the transition occurred at a perimeter of ~19 μm during all first four divisions (Figures 2A and 2B), indicating that it is controlled by a mechanism that is independent of initial ring size.

One mechanism that could account for the size independence of the transition is proximity of the constricting ring to the spindle midzone, a set of microtubule bundles that forms between the separating chromosomes during anaphase. The dimensions of the spindle midzone are determined by the segregating chromosome masses and are independent of initial cell size. To test this idea, we monitored constriction kinetics after depleting SPD-1, a microtubule bundling protein that is required for midzone bundle formation but does not prevent ring constriction (Verbrugghe and White, 2004; Figure 2C). We chose the 4→8 cell stage because the transition occurs about halfway through constriction during this division. The transition from constant to decreasing closure rate did not occur in the SPD-1-depleted embryos, and the ring closed at a constant rate to completion (Figure 2D). These results indicate that the contractile ring has the potential to close at a constant rate to completion, but this intrinsic property is modulated when the spindle midzone is present. This explanation accounts for the differing relative contributions of the two phases: in large cells, the contractile ring closes at a constant rate for a larger percentage of constriction before encountering the midzone; as cell size decreases, the contractile ring forms in proximity to the spindle midzone, leading to constriction at a rate that decreases in proportion to perimeter soon after constriction onset (Figure 2E).

Constant Constriction Rate Is Proportional to Initial Ring Size during the First Four Embryonic Divisions

The initial perimeter of the contractile ring is significantly greater during the early divisions than during the later divisions. By contrast, the time required for the ring to constrict from its initial perimeter to ~5 μm was remarkably similar for all five divisions (Figure 1G). The basis for this property is evident when the constant phase constriction rate is plotted versus initial perimeter—a clear proportionality is observed (Figure 3A). In addition, the linear fit relating the constant constriction rate to initial perimeter passes through the origin. Thus, if contractile rings closed to completion at a constant rate, all rings would close in the same amount of time irrespective of their initial size (closure time = $1/\alpha$, where α is the slope of the plot in Figure 3A). However, due to the transition triggered by midzone proximity, contractile rings do not close to completion at a constant rate (Figure 2). The midzone-dependent transition has two effects. First, the overall duration of cytokinesis includes the duration of the second phase, $\sim 1.386 P_{TP}/\alpha P_0$ (where P_0 and P_{TP} are the initial and transition perimeters, respectively; see Supplemental Data E for details), as well as that of the constant phase. Second, the duration of the constant phase is shortened to $1/\alpha - P_{TP}/\alpha P_0$ because the rings constrict at a constant rate to the transition perimeter and not to completion. Because the duration of the second phase and the reduction in the duration of the constant phase are both $\sim P_{TP}/\alpha P_0$, the time required to complete constriction differs only slightly from $1/\alpha$, which is what it would be if there were no midzone-dependent transition. Consequently, cytokinesis occurs in the same amount of time, independent of starting size. We note that because $P_{TP}/\alpha P_0$ is inversely proportional to initial perimeter, the relative contributions of the two phases do change with cell size; bigger cells take longer to reach the transition point but progress from the transition point to 5 μm more quickly, whereas smaller cells reach the transition point more quickly but take longer to go from the transition point to 5 μm (Figure 2E).

Our data indicate that the similar duration of cytokinesis is a consequence of the proportionality between the constant phase constriction rate and initial ring size. This inherent scalability of

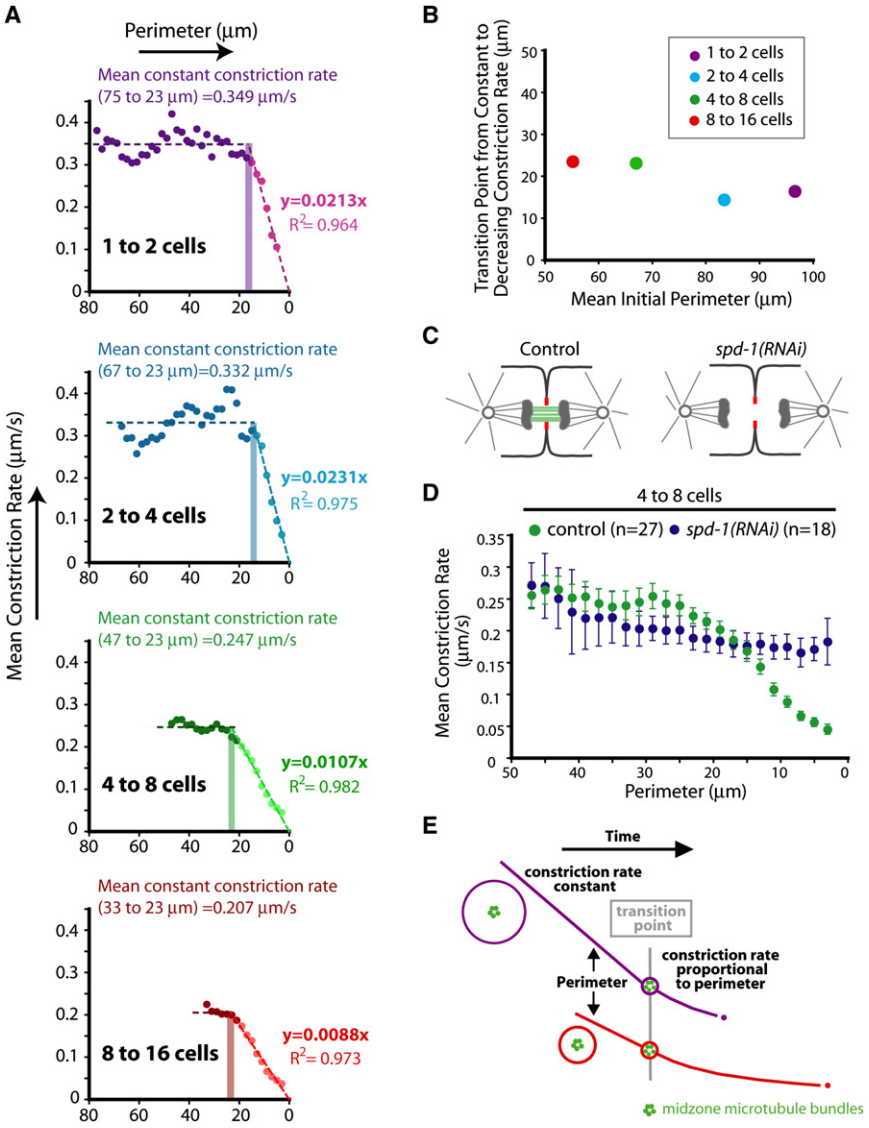

Figure 2. The Transition from Constant to Decreasing Constriction Rate Occurs at a Fixed-Ring Perimeter Controlled by the Spindle Midzone

(A) Mean constriction rate plotted versus perimeter as in Figure 1H. For clarity, the data for each division is shown separately and without error bars. The mean constant phase constriction rate, the linear equation used to fit the declining rate during the second phase, and the transition point (vertical bars) are shown on each graph.

(B) The transition point plotted versus mean initial perimeter for the first four divisions.

(C) Schematic illustrating the midzone microtubule bundles (green) and the constricting ring (red). SPD-1 is required for the stable bundling of midzone microtubules.

(D) Mean constriction rate plotted versus perimeter for the 4→8 cell division in control and *spd-1(RNAi)* embryos. Error bars, 95% CI.

(E) The contractile ring constricts in two phases. During the first phase, the constriction rate is constant and ring perimeter decreases linearly with time. During the second phase, the constriction rate decreases linearly in proportion to perimeter and ring perimeter decreases exponentially with time. The transition between the two phases requires midzone microtubule bundles and occurs at a fixed perimeter independent of initial ring size.

constant phase constriction is evident when the constriction rate per unit length is plotted versus decreasing perimeter for each division—the constriction rate per unit length progressively increases in proportion to the fold decrease in perimeter in a uniform fashion during all four divisions (Figure 3B).

Cumulatively, these results indicate that initial ring size determines the constriction rate throughout closure. Thus, the ability to retain a structural memory of its initial size is a fundamental mechanical property of the contractile ring that allows it to generate a barrier between the separated chromosomes in a similar time frame despite significant differences in starting size.

Constant Constriction Rate in the ABa Cell Is Proportional to Initial Ring Size When Embryo Size Is Varied

The constant phase constriction rate decreases in proportion to cell size during the first four embryonic divisions. However, developmental regulation or the presence of additional resistive forces resulting from the formation of new cell-cell contacts, instead of cell size, could underlie the observed scaling. To exclude these alternatives, we examined how constriction scales with respect to initial cell perimeter within the context of a single cell division—the ABa division at the four-cell stage. We experimentally altered ABa cell perimeter using RNAi of the gonad-specific anillin homolog *ani-2*, which broadens the size distribution for the brood of embryos laid by the treated worm (Maddox et al., 2005). Effectively, *ani-2(RNAi)* makes it possible to vary cell size, while keeping the developmental stage, cell geometry, and proportion of the surface in contact with other cells constant. The embryos laid by *ani-2(RNAi)* mothers were partitioned into three groups based on initial ABa cell perimeter, and the mean initial perimeter and mean constriction rate during the constant phase were determined for each group (Figures 3C–3E). This analysis revealed a linear proportionality between the constant phase constriction rate and initial cell perimeter that was very similar to that observed for the first four divisions in wild-type. These results strongly support the conclusion that the decrease in the constant closure rate during the first four embryonic divisions is due to the decrease in cell size.

Concentration of Three Structural Components of the Contractile Ring Remains Constant during Constriction

During the first phase of closure, constriction occurs at a constant rate as the ring decreases between 2-fold (16→32 cells) and

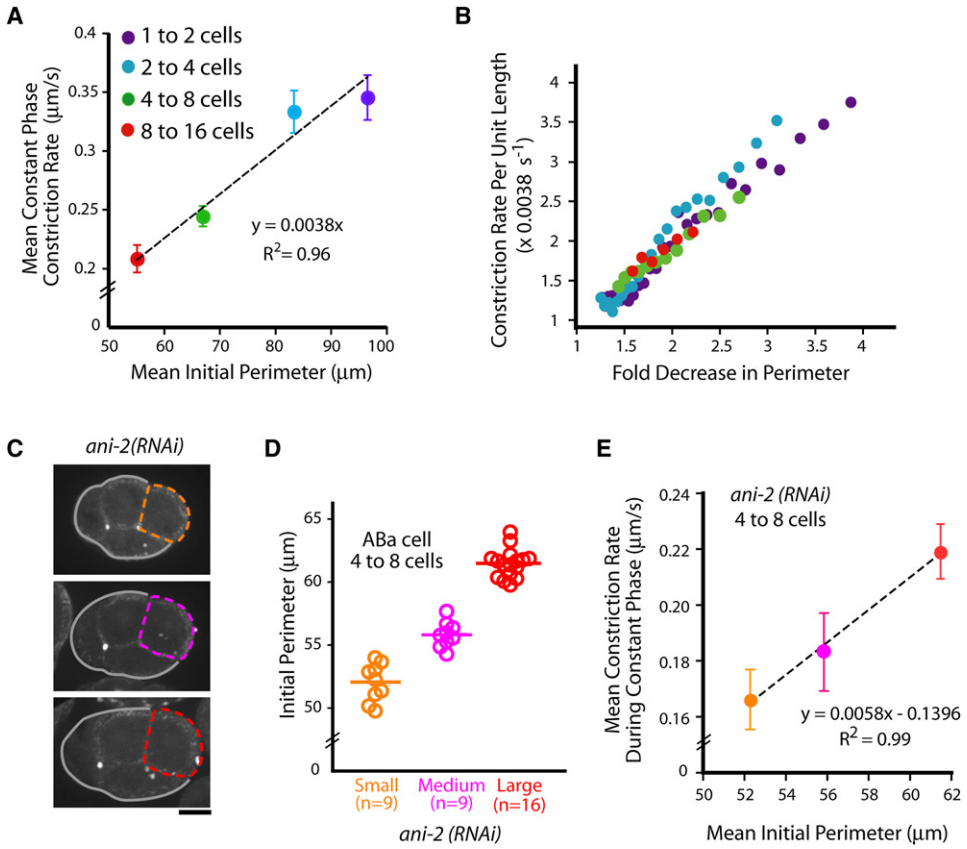

Figure 3. The Constriction Rate during the Constant Phase of Contractile Ring Closure Is Proportional to the Initial Ring Size

(A) Mean constant phase constriction rate plotted versus mean initial perimeter for the first four divisions (1→2: n = 98 measurements in 9 embryos; 2→4: n = 98 measurements in 13 embryos; 4→8: n = 134 measurements in 27 embryos; 8→16: n = 37 measurements in 10 embryos).

(B) Mean constriction rate per unit length is plotted versus fold decrease in perimeter for the first four divisions.

(C) Confocal images of small (top) to large (bottom) *ani-2(RNAi)* embryos expressing NMY-2-GFP. Scale bar, 10 μm.

(D) The distribution of initial ABa cell perimeters is shown for the small, medium, and large *ani-2(RNAi)* embryos, with the horizontal bar representing the mean.

(E) Mean constant phase constriction rate plotted versus mean initial perimeter for the small, medium, and large embryos defined in (D) (based on 64, 66, and 98 measurements in 9 small, 9 medium, and 16 large embryos, respectively). Error bars, 95% CI.

5-fold (1→2 cells) in size. To sustain the constant constriction rate, the constriction rate per unit length increases in proportion to the fold decrease in perimeter (Figure 3B). One mechanism to achieve this would be to keep the total amount of the motor-driving movement in the ring constant as the ring decreases in size, leading to an increase in motor concentration and in the amount of force the motor generates per unit length. To test whether such a mechanism was operating, we monitored the fate of myosin II (NMY-2) along with two other structural components of the ring—the septins (UNC-59) and anillin (ANI-1)—during constriction.

We analyzed the amount of myosin, the septins, and anillin in the ring in the ABa cell at the 4→8 cell stage because ring constriction in this cell is partitioned evenly between the two phases, allowing the fate of components to be monitored during both phases. The NMY-2-GFP and GFP-UNC-59 fusions rescue mutations in the corresponding genes, confirming their functionality (Supplemental Data F and G); due to lack of a mutant, the functionality of the GFP-ANI-1 fusion has not been tested. During the ABa cell division, the contractile ring appears triangular, consisting of two "sides" where ABa contacts its two neighboring cells and a free circular arc that ingresses from the periphery toward the embryo center. All three probes concentrate in the contractile ring at the leading edge of the ingressing furrow. By contrast, the $RFP^{mCherry}$ probe, which is a fusion with a pleckstrin homology (PH) domain that binds to the phosphoinositide lipid PI4,5P2, is not enriched in the contractile ring (Figures 4A–4C and Movie S3).

We quantified the fluorescence of each probe in the free arc throughout constriction (Figure 4D and Supplemental Data H). This analysis revealed that the GFP fluorescence per unit length remained constant during the majority of constriction for all three probes, with only a slight increase at the end, when the perimeter became smaller than 10 μm. This increase was most pronounced for GFP-anillin, which increased ~1.3-fold in concentration as the ring perimeter decreased from ~18 to 5 μm during the second phase of constriction. To increase the dynamic range over which constant rate constriction can be monitored, we repeated our analysis in *spd-1(RNAi)* embryos (Figure 2D) and found that the concentration of all three markers remained between 0.8-fold

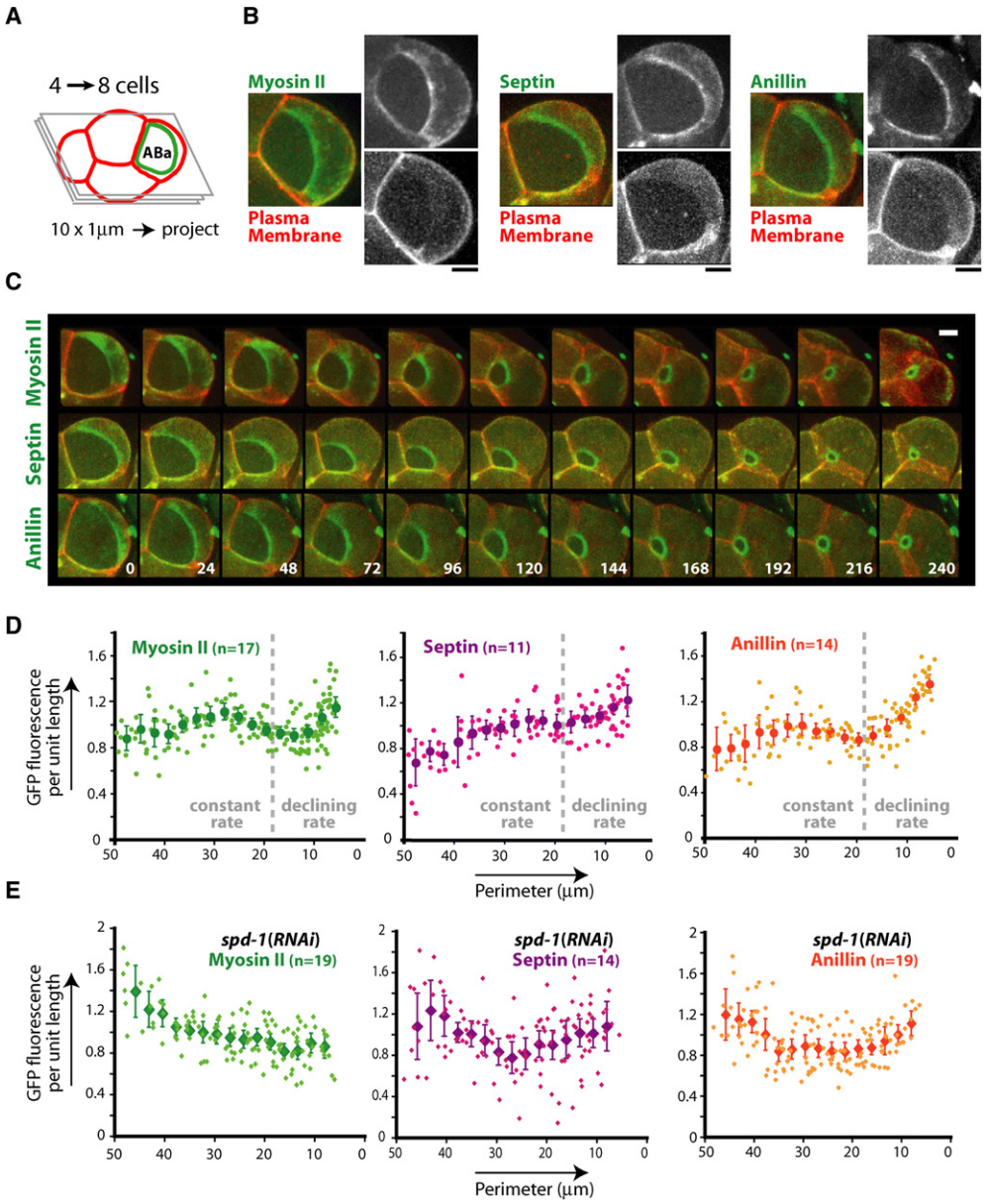

Figure 4. The Concentration of Three Structural Components of the Contractile Ring Remains Constant during Constriction

(A) The dynamics of contractile ring components were analyzed on maximum intensity projections of 10 × 1 μm z-series acquired in the ABa cell at the four-cell stage.

(B) Images of the contractile ring in the ABa cell in embryos coexpressing an $RFP^{mCherry}$-labeled plasma membrane probe along with NMY-2-GFP, GFP-UNC-59, or GFP-ANI-1.

(C) Time-lapse sequences of constricting contractile rings in the ABa cell of embryos coexpressing the $RFP^{mCherry}$-labeled plasma membrane probe and the GFP-labeled contractile ring probes. Time is in seconds.

(D and E) Plots of GFP fluorescence per unit length versus perimeter in control (D) or *spd-1(RNAi)* embryos (E) expressing NMY-2-GFP, GFP-UNC-59, or GFP-ANI-1. Smaller dots represent individual measurements normalized to the mean GFP intensity of the measurements in that embryo. The larger data points are the mean of measurements falling in overlapping 6 μm intervals plotted against the perimeter at the center of each interval. Error bars, 95% CI; scale bars, 5 μm.

and 1.2-fold of the average value over a 5-fold change in perimeter, from 50 to 10 μm (Figure 4E). Measurement of contractile ring width (Supplemental Data I–K) and thickness (Supplemental Data L) indicated that they do not change during constriction. We conclude that the amount per unit length of the motor myosin II as well as two structural components (the septins and anillin) does not change during constant rate constriction even though the rate of closure per unit length increases. Thus, myosin, the septins, and anillin all behave in an essentially identical fashion, with the total amount of each component in the ring decreasing

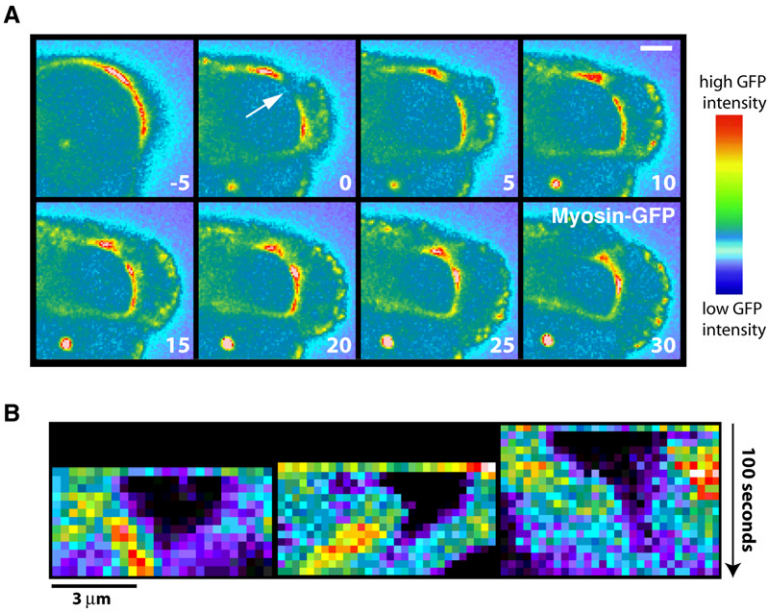

Figure 5. Myosin in the Contractile Ring Does Not Exchange Rapidly with Cytoplasmic or Cortical Pools during Constriction

(A) A region of the contractile ring in an embryo expressing NMY-2-GFP was photobleached (arrow) and followed over time. Time is in seconds after photobleaching. Stills are in pseudocolor with hot-to-cold colors representing high-to-low GFP intensity. Scale bar, 5 μm.

(B) Kymographs of the bleached region as illustrated in (C). The time interval between each row of pixels is 5 s. The top row corresponds to the time point before photobleaching. Pixel dimensions are 0.27 × 0.27 μm.

(C) For quantification, a box of constant width was drawn over a portion of the GFP arc containing the bleached and flanking regions.

(D) Mean GFP fluorescence per unit length plotted versus time. Smaller dots represent individual data points normalized to the average GFP signal within the box prior to photobleaching. Larger dots are the mean of the normalized GFP intensity measurements falling in overlapping 10 s intervals plotted against the time at the center of each interval. Error bars, 95% CI.

in proportion to the decrease in ring perimeter, indicating that constriction is coupled to progressive disassembly of the contractile ring.

Myosin in the Contractile Ring Does Not Exchange Rapidly with Cytoplasmic or Cortical Pools during Constriction

The total amount of myosin, septins, and anillin in the contractile ring decreases during constriction in proportion to the decrease in ring perimeter. This decrease could be achieved by incorporation into the ring during assembly and progressive loss during constriction or by rapid turnover in combination with a decrease in the number of binding sites as the ring gets smaller. To distinguish between these possibilities, we performed fluorescence recovery after photobleaching (FRAP) experiments in strains expressing NMY-2-GFP (Figure 5 and Supplemental Data M) and GFP-UNC-59 (Supplemental Data N). We generated kymographs to monitor the fate of the bleached region for both markers and quantified the recovery of NMY-2-GFP by measuring the average GFP signal per unit length within a curved box of constant width that included the bleached and flanking unbleached areas (Figure 5C). If myosin and septins in the contractile ring were exchanging rapidly with the cytoplasmic or cortical pools, the GFP signal in the bleached region should rapidly recover along its entire length. Alternatively, if there were only constriction-coupled disassembly, the recovery should be slow and the bleached region should get progressively smaller as constriction proceeded. Kymographs of the bleached regions for both NMY-2-GFP (Figure 5B) and GFP-UNC-59 (Supplemental Data N) exhibited a tornado shape, indicating that the bleached regions do not recover uniformly along their entire length due to rapid exchange with cytoplasmic or cortical pools, but instead progressively fill in from their ends. Quantification of the NMY-2-GFP signal supported this conclusion; instead of rapidly returning to its initial level, the NMY-2-GFP fluorescence per unit length only recovered to a small extent (Figure 5D). If filling in of the photobleached regions resulted exclusively from ring constriction, then over a 95 s interval, the gap should decrease by 50% in length. Instead, the gaps decreased in length more rapidly, typically disappearing within 60–90 s (Figure 5B and Supplemental Data N). This result suggests that, although there does not appear to be much exchange of the myosin and septins in the contractile ring with cytoplasmic or cortical pools, there may be some lateral mobility of both components within the contractile ring. The lack of rapid turnover is consistent with the idea that the contractile ring is initially built and progressively disassembled in a manner that allows it to have a structural memory and complete constriction in a similar time frame regardless of initial size.

Contractile Ring Constriction Continues If Latrunculin A Is Added after Constriction Onset

The scaling of cytokinesis with cell size and the behavior of myosin and the septins suggests that the contractile ring is initially built and subsequently progressively disassembled without continuous turnover of its structural components. Because the formin-nucleated actin filaments in the contractile ring do not incorporate either GFP or chemically labeled actin subunits, we have been unable to directly test whether actin

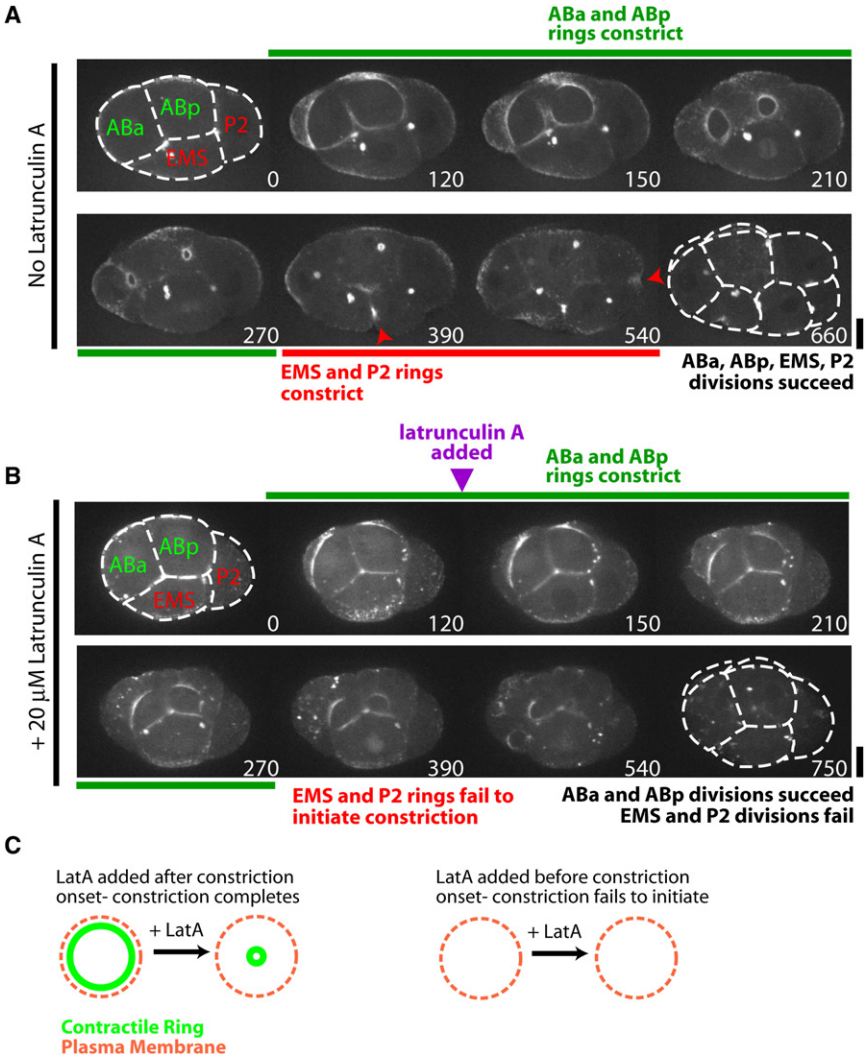

Figure 6. Ring Constriction Continues If Latrunculin A Is Added after Constriction Onset

(A and B) Control (A) and latrunculin A-treated (B) four-cell-stage embryos expressing NMY-2-GFP. In the control embryo (A), EMS and P2 initiated cleavage ~240 s after ABa and ABp. In the embryo in (B), latrunculin A was added at the four-cell stage immediately after the contractile ring in the ABa and ABp cells initiated constriction (120 s). The rings in ABa and ABp continued to close to completion over the following 500 s, whereas the EMS and P2 cells, which normally begin constriction ~240 s after ABa and ABp, failed to initiate cleavage. Scale bar, 10 μm.

(C) Schematic summarizing the consequences of latrunculin A addition after and prior to constriction onset.

filaments are rapidly turning over. To analyze actin dynamics, we therefore took a different approach—acute treatment with latrunculin A after constriction onset (Figure 6). Latrunculin A prevents filament assembly by binding free actin monomer but does not affect existing filaments. If constriction required rapid actin turnover, latrunculin A treatment should immediately stop ingression. Conversely, if actin filaments are assembled as the ring forms and then progressively shortened during constriction, latrunculin A treatment should not stop ingression. To distinguish between these outcomes, we performed acute latrunculin A treatments on the first-to-divide cell(s) at the two-cell (AB) or four-cell stages (ABa and ABp, which initiate constriction simultaneously). The natural developmental asynchrony of the *C. elegans* embryo allowed the adjacent cells (P1 at the two-cell stage; EMS and P2 at the four-cell stage), which initiate cleavage shortly thereafter, to serve as internal controls; if the treatment was successful, these cells should not assemble a contractile ring and initiate cytokinesis. Precisely timed drug addition is difficult in the *C. elegans* embryo because of the impermeable eggshell and the rapidity of the early divisions but, by adapting a protocol developed to remove the eggshell for blastomere cultures (Edgar, 1995), we obtained unambiguous results on seven cells from four embryos. In all seven cells where we were successful at introducing the drug immediately after constriction onset, the ring continued to constrict even though the adjacent P1 (two-cell stage) and EMS/P2 (four-cell stage) cells in the same embryos exhibited no sign of contractile ring assembly (Figures 6B and 6C and Movie S4). Cortical regions away from the contractile ring in the analyzed cells also exhibited clear abnormalities, confirming efficacy of the drug. Six of the seven cells successfully completed cytokinesis; in the remaining cell, the ring completed the majority of constriction but the point of connection with the adjacent cell (ABp) lost integrity and caused it to open back up. We note that, within the limited number of observed cells, the constriction rate of the latrunculin A-treated rings was slightly slower than that of similarly treated controls (closure completed in 380-600 s versus ~300 s for controls). It is not clear why the constriction rate is slower, but we suspect this may be due to defects in cortical integrity outside the ring. We conclude that rapid actin turnover is not required for constriction. Instead, our results suggest that actin filaments are assembled as the ring forms and then progressively shorten during constriction.

DISCUSSION

Contractile Ring Inherently Constricts at a Constant Rate, but This Property Is Modulated by the Spindle Midzone

During the early *C. elegans* embryonic divisions, contractile ring constriction occurs in two phases. The transition from constant to decreasing constriction rate occurs at a fixed-ring perimeter

in all divisions and requires an intact spindle midzone (Figure 2E). The constriction rate may slow as the contractile ring comes into proximity to the spindle midzone due to a physical barrier or to signaling by the microtubule bundles. We speculate that slowing constriction contributes to the cytokinesis fidelity—communication between the spindle midzone and the contractile ring late in constriction could ensure that the ring closes precisely around the microtubule bundles at the midpoint between the separated chromosomes.

Our experiments indicate that the contractile ring has the potential to close at a constant rate to completion. This conclusion runs counter to a previous model, which postulated that constriction cannot complete at a constant rate due to a progressive increase in actin filament density (Biron et al., 2005). Closure at a constant rate has been documented in lower eukaryotes, including *S. pombe* (Pelham and Chang, 2002), the amoeba *E. invadens*, and, under some conditions, *Dictyostelium discoideum* (Biron et al., 2004). Thus, the intrinsic ability to close at a constant rate is a broadly conserved feature of the contractile mechanism, which in animal cells is modulated by proximity to the spindle midzone.

Constancy of Contractile Ring Structure during Constriction

Our analysis reveals that component concentration in the contractile ring, as well as ring width and thickness, remain constant as the perimeter decreases, despite the increase in constriction rate per unit length. These findings exclude the possibility that an increase in the concentration of the force-generating motor myosin II is responsible for the increase in constriction rate per unit length during the constant phase. In contrast to *C. elegans* embryos, in *S. pombe*, myosin II increases in concentration in proportion to the decrease in perimeter (Wu and Pollard, 2005). Ring closure in *S. pombe* is ~40× slower (~0.5 μm/min versus ~20 μm/min during the first division of the *C. elegans* embryo), occurs over a significantly smaller distance (~10 μm in *S. pombe* versus 100 μm during the first division of the *C. elegans* embryo), and is coupled to synthesis of cell wall material to form a septum. These factors may underlie the observed difference.

The photobleaching analysis indicates that myosin II in the ring exhibits little or no exchange with cortical or cytoplasmic pools during constriction. This result is consistent with the idea that the contractile ring is built and progressively disassembled during constriction, and is in marked contrast to the currently prevalent idea that contractile ring components turn over rapidly relative to the constriction rate. In *S. pombe*, Cdc4p (the myosin II essential light chain) and Cdc8p (the actin-associated protein tropomyosin) both turn over rapidly ($t_{1/2}$ = 20–30 s) in the contractile ring (Pelham and Chang, 2002), which may reflect a difference in the dynamics of contractile ring components between *C. elegans* and fission yeast. Alternatively, the dynamics of Cdc4p and Cdc8p may not reflect those of the underlying myosin and actin filaments, or, because the fission yeast photobleaching study was performed prior to constriction, the onset of constriction may bring about a change that renders ring components less dynamic.

We have been unable to monitor actin dynamics in *C. elegans* because the formin-nucleated actin filaments in the contractile ring do not incorporate either GFP or chemically labeled actin subunits (unpublished data), consistent with a prior report in *S. pombe* (Wu and Pollard, 2005). Rapid turnover has been reported for labeled actin in the cleavage furrow of cultured vertebrate cells (Murthy and Wadsworth, 2005; Guha et al., 2005). The measured half-time for recovery (~30 s) is similar to that reported for Arp2/3-nucleated actin arrays (Theriot and Mitchison, 1991; Theriot et al., 1992). This similarity, coupled with the difficulty of incorporating labeled subunits into formin-nucleated filaments, leads us to suspect that the rapid dynamics observed in prior work represents Arp2/3-nucleated actin in the furrow region and not the formin-nucleated actin filaments in the contractile ring. Based on our analysis of component fates and turnover during constriction, the structural memory of initial ring size, and the results of latrunculin A treatment after constriction onset, we propose that the contractile ring is not turning over rapidly but is instead progressively disassembled in a constriction-coupled manner.

A Model to Explain Structural Memory in the Contractile Ring

Our results indicate that there is built-in scalability of contractile ring constriction. This scalability arises from the proportionality between the constant phase constriction rate and initial ring size (Supplemental Data E). To explain this structural memory as well as the constant closure rate, we propose a model (Figure 7) based on three assertions: (1) a series of contractile units are incorporated into the ring at the time of its assembly; (2) the contractile units are of fixed size so that larger rings contain a proportionally greater number of units than smaller rings; and (3) during constriction, each unit shortens at the same constant rate, causing larger rings composed of more units to constrict at a proportionally faster constant rate than smaller rings composed of fewer units. A key aspect of this model is that the decrease in ring perimeter is accomplished by unit shortening rather than by loss of units. This "contractile unit" model explains the structural memory as well as the constant constriction rate during the first phase of ring closure and is consistent with our data on contractile ring component dynamics.

Two important questions raised by the proposed model are the nature of the putative contractile units and the mechanism of their shortening. EM performed on cultured HeLa cells (Maupin and Pollard, 1986) and on cleavage furrows isolated from newt embryos (Mabuchi et al., 1988) suggested that the actin filaments in the contractile ring are organized into small bundles, which could represent the contractile units (incorporated into the model in Figure 7B). Within the bundles, the actin filaments appeared to be interdigitated with thicker filaments that, based on their dimensions, could be filaments of myosin II. Maupin and Pollard (1986) found that during constriction, neither the diameter of the bundles nor the number of filaments in the bundles (counted in cross-section) changed substantially. Based on these results, they proposed that the individual actin filaments that make up the bundles shorten during constriction, most likely without being lost. The results of latrunculin A treatment after constriction onset that we report here support the idea that actin filaments assemble when the ring forms and then progressively shorten during constriction.

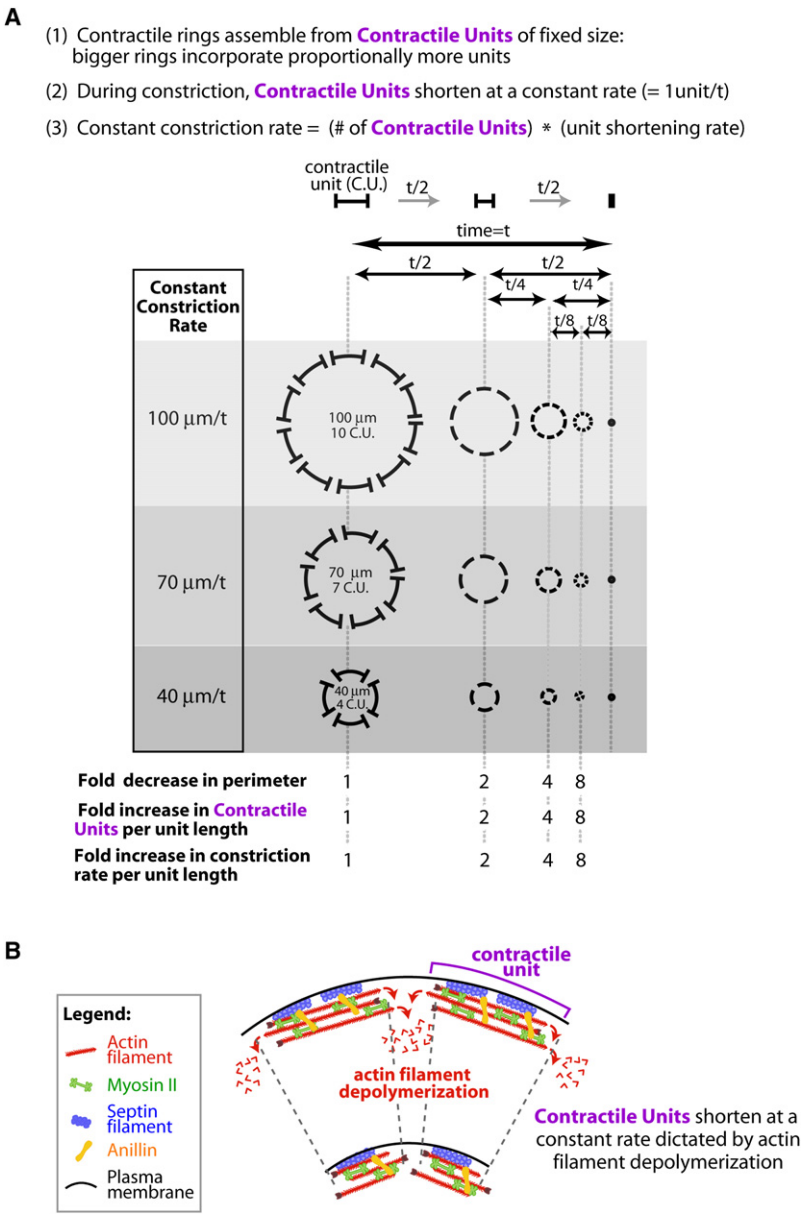

Figure 7. Model for Contractile Ring Structure and Constriction

(A) A "contractile unit" model explains the proportionality between initial ring size and constant phase constriction rate as well as the ability of the ring to retain structural memory of its initial size as it disassembles. In this model, contractile rings assemble from contractile units of fixed size. Consequently, bigger rings incorporate proportionally more units. During constriction, each unit shortens at a constant rate, so initially larger rings composed of more units constrict at a proportionally faster constant rate than smaller rings composed of fewer units. This organization renders constriction perfectly scalable; the duration of constriction is independent of initial ring size and depends only on the unit-shortening properties. We illustrate this schematically for rings of three initial sizes that constrict at a constant rate to completion assuming a single layer of units with a hypothetical length of 10 µm. (B) Schematic representation of the putative contractile unit as a bundle of actin filaments interdigitated with bipolar filaments of the motor myosin II. The rate of contractile unit shortening is dictated by the rate of actin filament depolymerization, which reduces the number of binding sites for myosin II, anillin, and the septins. Because the number of actin filaments in the bundle remains constant, contractile units maintain a constant rate of shortening despite their decreasing length.

Our model proposes that the constant constriction rate is derived from the constant shortening rate of individual contractile units. An attractive mechanism to explain this property of the units is actin filament depolymerization. Actin filaments shorten from their ends at a constant rate that is independent of their length. Thus, coupling unit shortening to actin filament depolymerization would explain how the contractile ring maintains a constant constriction rate despite its decreasing circumference (Figure 7B). We note that actin filament depolymerization could limit the constriction rate irrespective of whether depolymerization itself (Dogterom and Yurke, 1997; Mogilner and Oster, 2003; Dickinson et al., 2004; Zumdieck et al., 2007) or an actin-myosin sliding filament-type mechanism provides the force that drives constriction.

Our model predicts the presence of "unit delimiters"—components whose total amount scales with the number of units in the ring rather than ring perimeter. Such unit delimiters should exhibit a behavior different from that which we document here for myosin II, the septins, and anillin—they should stay constant in amount, and therefore increase in concentration during constriction. Potential candidates for the unit delimiters include the formins or proteins that cap the ends of actin filaments and/or act as end-tracking crosslinkers.

In summary, we have demonstrated that the contractile ring exhibits a remarkable property that renders the time required for constriction independent of the initial size. Biologically, this is likely to be very important. During the successive divisions that partition the egg cytoplasm during embryogenesis, the dimensions of the chromosomes remain constant, whereas the distance that the contractile ring needs to traverse to reach them varies with each division. The mechanism we outline here would allow the ring to reach the midpoint between the chromosomes in the same amount of time irrespective of the initial size of the ring, thereby coordinating cell cycle progression with cytokinesis.

EXPERIMENTAL PROCEDURES

C. elegans Strains

Strain genotypes are listed in Table S1. Strains coexpressing GFP-labeled contractile ring markers along with the $RFP^{mCherry}$ plasma membrane probe

were generated by mating OD70 (Kachur et al., 2008) to JJ1473 (NMY-2-GFP; Nance et al., 2003), OD26 (GFP-UNC-59; Maddox et al., 2007), or OD38 (GFP-ANI-1; Maddox et al., 2007), respectively. Strains expressing GFP-ANI-1 were kept at 25°C. All other strains were kept at 20°C. Latrunculin A treatment was performed as described in Supplemental Data O.

RNA Interference

dsRNAs were prepared as described (Oegema et al., 2001) using the primer pairs (5′-TAATACGACTCACTATAGGTCGTTGACGCGTACTCAACT-3′ and 5′-AATTAACCCTCACTAAAGGGAATTCGAAATCCGACTCCA-3′) and (5′-TAATACGACTCACTATAGGGAGACCACCAACGACTCCAAACGTCAGATA-3′ and 5′-AATTAACCCTCACTAAAGGGTCTCGTCCGTTTCTTGTTTCT-3′) to amplify regions of *spd-1 or ani-2*, respectively, from N2 genomic DNA. After RNA injection, L4 worms were incubated for 42–46 hr at 20°C prior to filming their embryos.

Live Imaging

Embryos were mounted as previously described (Oegema et al., 2001) and imaged at 21°C using a 60× 1.4 NA PlanApochromat lens on a spinning disk confocal mounted on a Nikon TE2000-E inverted microscope equipped with a krypton-argon 2.5 W water-cooled laser (Spectra-Physics, Mountain View, CA) and either an electron multiplication back-thinned charge-coupled device camera (iXon; Andor Technology) or a Hamamatsu Orca ER CCD camera. Acquisition parameters, shutters, and focus were controlled by MetaMorph software (Molecular Devices, Downington, PA). Exposure times were 100 and 200 ms for GFP and RFP images, respectively (laser power = 0.8 W). For FRAP experiments, the 488 nm laser line was steered into a custom-modified epifluorescence port, creating a spot with a full width at half-max of 800 nm in the objective focal plane. The exposure time for the bleach was 50 ms (laser power = 0.8 W).

Measurement of Contractile Ring Perimeter and Constriction Rate

During the 1→2 and 2→4 cell divisions, an 11 × 2.5 μm GFP z-series was collected every 20 s, and contractile ring perimeters were calculated from the maximum measured diameter. During the 4→8, 8→16, and 16→32 cell divisions, a 10 × 1 μm GFP/RFP z-series was collected every 24 s, and contractile ring perimeter was measured by manually tracing the outline of the contractile ring in maximum intensity projections of the z-stacks. Data from multiple embryos were pooled, averaged, and time aligned with respect to the initial deformation of the cortex. The rate of constriction was calculated for pairs of consecutive time points by dividing the difference in perimeter by the time interval. Graphs of the mean rate of constriction versus perimeter were generated by pooling the individual rate measurements from all imaged embryos and plotting the mean rate for the data points falling in overlapping 6 μm intervals against the perimeter at the center of each interval.

Measurement of GFP Fluorescence in the Contractile Ring

The mean GFP fluorescence per unit length was quantified in maximum intensity projections by drawing a curved box of constant width over the arc, avoiding the cell-cell contacts, for each time point and subtracting the mean background fluorescence (measured in a 10 pixel diameter circle drawn over the cytoplasm in the center of the ring). Data from multiple embryos were pooled to generate plots of GFP fluorescence per unit length versus perimeter after normalizing individual measurements by dividing by the mean GFP intensity for the series of measurements made in that embryo.

Measurement of Myosin II Turnover

A portion of the NMY-2-GFP contractile ring (~3–4 μm in length) was photobleached, and 3 × 0.5 μm z-series were collected every 5 s before and after the bleach. Maximum projections were generated and a box of variable length and constant width was drawn over the GFP arc encompassing the bleached region and the flanking regions for each time point. The mean GFP fluorescence per unit length within the box was quantified, and the mean background fluorescence (measured in a 10 pixel diameter circle drawn over the cytoplasm in the center of the ring) was subtracted. Data points from 14 bleached embryos were pooled after normalizing the values within each series by dividing by the average GFP signal within the box prior to photobleaching.

SUPPLEMENTAL DATA

Supplemental Data include sixteen figures, four movies, and one table and can be found with this article online at http://www.cell.com/supplemental/S0092-8674(09)00320-1.

ACKNOWLEDGMENTS

We thank our reviewers for providing challenging feedback that greatly improved the manuscript; Craig Mello and Ji Liu for the unpublished strain WM179; Chris Campbell and Reto Gassmann for critical reading of the manuscript; and members of the Oegema and Desai labs for support. A.C. was funded by the Fundação para a Ciência e Tecnologia, Portugal, and the European Social Fund (SFRH/BPD/26519/2006). K.O. is a Pew Scholar in the Biomedical Sciences. K.O. and A.D. receive salary and additional support from the Ludwig Institute for Cancer Research.

Received: September 1, 2008
Revised: December 30, 2008
Accepted: March 11, 2009
Published: May 28, 2009

REFERENCES

Arnold, J.M. (1969). Cleavage furrow formation in a telolecithal egg (Loligo pealii). I. Filaments in early furrow formation. J. Cell Biol. *41*, 894–904.

Biron, D., Libros, P., Sagi, D., Mirelman, D., and Moses, E. (2004). Biphasic cytokinesis and cooperative single cell re-production. In Forces, Growth and Form in Soft Condensed Matter: At the Interface between Physics and Biology, A.T. Skjeltorp and A.V. Belushkin, eds. (Berlin: Springer), pp. 217–234.

Biron, D., Alvarez-Lacalle, E., Tlusty, T., and Moses, E. (2005). Molecular model of the contractile ring. Phys. Rev. Lett. *95*, 098102.

Dickinson, R.B., Caro, L., and Purich, D.L. (2004). Force generation by cytoskeletal filament end-tracking proteins. Biophys. J. *87*, 2838–2854.

Dogterom, M., and Yurke, B. (1997). Measurement of the force-velocity relation for growing microtubules. Science *278*, 856–860.

Edgar, L.G. (1995). Blastomere culture and analysis. Methods Cell Biol. *48*, 303–321.

Eggert, U.S., Mitchison, T.J., and Field, C.M. (2006). Animal cytokinesis: from parts list to mechanisms. Annu. Rev. Biochem. *75*, 543–566.

Field, C.M., Maddox, A., Pringle, J.R., and Oegema, K. (2008). Septins in the metazoan model systems Drosophila melanogaster and Caenorhabditis elegans. In The Septins, P.A. Hall, S.E. Hilary Russell, and J.R. Pringle, eds. (New York: John Wiley & Sons), pp. 147–168.

Guha, M., Zhou, M., and Wang, Y. (2005). Cortical actin turnover during cytokinesis requires myosin II. Curr. Biol. *15*, 732–736.

He, X., and Dembo, M. (1997). On the mechanics of the first cleavage division of the sea urchin egg. Exp. Cell Res. *233*, 252–273.

Kachur, T.M., Audhya, A., and Pilgrim, D.B. (2008). UNC-45 is required for NMY-2 contractile function in early embryonic polarity establishment and germline cellularization in *C. elegans*. Dev. Biol. *314*, 287–299.

Kamasaki, T., Osumi, M., and Mabuchi, I. (2007). Three-dimensional arrangement of F-actin in the contractile ring of fission yeast. J. Cell Biol. *178*, 765–771.

Kruse, K., and Jülicher, F. (2000). Actively contracting bundles of polar filaments. Phys. Rev. Lett. *85*, 1778–1781.

Kruse, K., and Jülicher, F. (2003). Self-organization and mechanical properties of active filament bundles. Phys. Rev. E Stat. Nonlin. Soft Matter Phys. *67*, 051913.

Kruse, K., Camalet, S., and Jülicher, F. (2001). Self-propagating patterns in active filament bundles. Phys. Rev. Lett. *87*, 138101.

Mabuchi, I. (1994). Cleavage furrow: timing of emergence of contractile ring actin filaments and establishment of the contractile ring by filament bundling in sea urchin eggs. J. Cell Sci. *107*, 1853–1862.

Mabuchi, I., Tsukita, S., Tsukita, S., and Sawai, T. (1988). Cleavage furrow isolated from newt eggs: contraction, organization of the actin filaments, and protein components of the furrow. Proc. Natl. Acad. Sci. U.S.A. *85*, 5966–5970.

Maddox, A.S., Habermann, B., Desai, A., and Oegema, K. (2005). Distinct roles for two *C. elegans* anillins in the gonad and the early embryo. Development *132*, 2837–2848.

Maddox, A.S., Lewellyn, L., Desai, A., and Oegema, K. (2007). Anillin and the septins promote asymmetric ingression of the cytokinetic furrow. Dev. Cell *12*, 827–835.

Maupin, P., and Pollard, T.D. (1986). Arrangement of actin filaments and myosin-like filaments in the contractile ring and of actin-like filaments in the mitotic spindle of dividing HeLa cells. J. Ultrastruct. Mol. Struct. Res. *94*, 92–103.

Mogilner, A., and Oster, G. (2003). Force generation by actin polymerization II: the elastic ratchet and tethered filaments. Biophys. J. *84*, 1591–1605.

Murthy, K., and Wadsworth, P. (2005). Myosin-II-dependent localization and dynamics of F-actin during cytokinesis. Curr. Biol. *15*, 724–731.

Nance, J., Munro, E., and Priess, J.R. (2003). *C. elegans* PAR-3 and PAR-6 are required for apicobasal asymmetries associated with cell adhesion and gastrulation. Development *130*, 5339–5350.

Oegema, K., Desai, A., Rybina, S., Kirkham, M., and Hyman, A.A. (2001). Functional analysis of kinetochore assembly in *Caenorhabditis elegans*. J. Cell Biol. *153*, 1209–1226.

Pelham, R.J., and Chang, F. (2002). Actin dynamics in the contractile ring during cytokinesis in fission yeast. Nature *419*, 82–86.

Sanger, J.M., and Sanger, J.W. (1980). Banding and polarity of actin filaments in interphase and cleaving cells. J. Cell Biol. *86*, 568–575.

Schroeder, T.E. (1968). Cytokinesis: filaments in the cleavage furrow. Exp. Cell Res. *53*, 272–276.

Schroeder, T.E. (1970). The contractile ring. I. Fine structure of dividing mammalian (HeLa) cells and the effects of cytochalasin B. Z. Zellforsch Mikrosk. Anat. *109*, 431–449.

Schroeder, T.E. (1972). The contractile ring. II. Determining its brief existence, volumetric changes, and vital role in cleaving Arbacia eggs. J. Cell Biol. *53*, 419–434.

Schroeder, T.E. (1975). Dynamics of the contractile ring. In Molecules and Cell Movement, R.E. Stephens and S. Inoué, eds. (New York: Raven Press), pp. 305–334.

Selman, G.G., and Perry, M.M. (1970). Ultrastructural changes in the surface layers of the newt's egg in relation to the mechanism of its cleavage. J. Cell Sci. *6*, 207–227.

Takiguchi, K. (1991). Heavy meromyosin induces sliding movements between antiparallel actin filaments. J. Biochem. *109*, 520–527.

Tanaka-Takiguchi, Y., Kakei, T., Tanimura, A., Takagi, A., Honda, M., Hotani, H., and Takiguchi, K. (2004). The elongation and contraction of actin bundles are induced by double-headed myosins in a motor concentration-dependent manner. J. Mol. Biol. *341*, 467–476.

Theriot, J.A., and Mitchison, T.J. (1991). Actin microfilament dynamics in locomoting cells. Nature *352*, 126–131.

Theriot, J.A., Mitchison, T.J., Tilney, L.G., and Portnoy, D.A. (1992). The rate of actin-based motility of intracellular Listeria monocytogenes equals the rate of actin polymerization. Nature *357*, 257–260.

Tucker, J.B. (1971). Microtubules and a contractile ring of microfilaments associated with a cleavage furrow. J. Cell Sci. *8*, 557–571.

Verbrugghe, K.J., and White, J.G. (2004). SPD-1 is required for the formation of the spindle midzone but is not essential for the completion of cytokinesis in *C. elegans* embryos. Curr. Biol. *14*, 1755–1760.

Wu, J.Q., and Pollard, T.D. (2005). Counting cytokinesis proteins globally and locally in fission yeast. Science *310*, 310–314.

Zumdieck, A., Kruse, K., Bringmann, H., Hyman, A., Jülicher, F., and Rutherford, S. (2007). Stress generation and filament turnover during actin ring constriction. PLoS ONE *2*, e696.